Available online at www.sciencedirect.com
ScienceDirect
International Journal of Mass Spectrometry 259 (2007) 79–86
International Journal of Mass Spectrometry
www.elsevier.com/locate/ijms

A novel surface-induced dissociation instrument for ion mobility-time-of-flight mass spectrometry

Wenjian Sun, Jody C. May, David H. Russell *

Laboratory for Biological Mass Spectrometry, Department of Chemistry, Texas A&M University, College Station, TX 77843, United States

Received 16 May 2006; received in revised form 31 August 2006; accepted 1 September 2006

Abstract

A surface-normal surface-induced dissociation (SID) configuration specifically designed for coupling ion mobility spectrometry (IMS) and orthogonal time-of-flight (TOF) mass spectrometer is described. The instrument configuration and the effects of various operating parameters are critically evaluated using ion trajectory calculations (SIMION) and SID spectra of a series of model peptides. The utility of the instrument configuration for simultaneous acquisition of MS and MS–MS spectra in both data-dependent and non-data-dependent modes are also discussed.

Keywords: Matrix assisted laser desorption/ionization; Surface-induced dissociation; Ion mobility; Time-of-flight

1. Introduction

Mass spectrometry (MS) has become an unrivaled technique for proteomics owing to high sample throughput and high mass measurement accuracy. The minimal amount of fragmentation observed by electrospray ionization (ESI) [1] and matrix-assisted laser desorption/ionization (MALDI) [2,3] greatly reduces spectral complexity. Furthermore, combining these ionization sources with tandem mass spectrometry allows for further characterization of analyte ions in terms of amino acid sequence of peptides and/or post-translational modifications (PTM) [4–6]. A variety of tandem mass spectrometry techniques have been developed for sequencing and PTM studies of peptides, the most frequently used being collision-induced dissociation (CID) [7–9]; however, surface-induced dissociation (SID) [10,11], photodissociation (PD) [12–14], electron capture dissociation (ECD) [15], and electron transfer dissociation (ETD) [16] have all demonstrated specific advantages over CID. In some cases SID is preferred over CID, because SID can be performed without the addition of a collision gas [11,28,29], which greatly simplifies the experiments, especially for high resolution TOF-MS and Fourier transform ion cyclotron resonance (FT-ICR)-MS, which require ultra-high vacuum for high resolution and accurate mass measurements.

SID was first introduced by Cooks in 1975 [10] and since that time a number of instrument configurations have been evaluated and the fundamentals of ion–surface collisions have been investigated. Especially relevant to SID are issues related to energy uptake by the ion–surface collisions [17–22]. Cooks recently published an excellent review that covers the fundamentals of SID and our current level of understanding of the SID process [23]. Of particular relevance for our work are the effects of surface-normal ion–surface interactions on energy uptake as well as the angle and kinetic energy distributions of the scattered ions.[24,25] Surface-normal SID has been previously performed by Laskin et al. using ion detection by FT-ICR-MS [24] and Zare and co-workers at the back of a reflector in a reflectron TOF-MS [26,27].

We previously described a MALDI-IM-SID-TOF instrument and discussed the advantages of coupling SID to IM-MS [30,31]. In this paper we describe a new SID instrument configuration, which greatly facilitates IM-SID-TOF-MS. This instrument has an SID region (a stainless steel ring electrode) that is positioned within the TOF ion source and SID is performed using a surface-normal incident angle. This design overcomes many of the limitations of the previous SID configurations, viz. low conversion efficiency of primary to secondary ions and inefficient collection of fragment ions, which significantly facilitates the

* Corresponding author at: P.O. Box 30012, Department of Chemistry, Texas A & M University, College Station, TX 77843, United States.
Tel.: +1 979 845 3345; fax: +1 979 845 9485.
E-mail address: russell@mail.chem.tamu.edu (D.H. Russell).

1387-3806/$ – see front matter © 2006 Elsevier B.V. All rights reserved.
doi:10.1016/j.ijms.2006.09.005

coupling of IMS with TOF while maintaining highly efficient energy deposition and subsequent fragment ion collection.

2. Experimental

The MALDI-IM-TOF instrument (Fig. 1) has been described previously [32]. Briefly, the MALDI ion source is equipped with a 20 Hz cartridge type nitrogen laser (337 nm, Thermo Laser Science), and a 30.5 cm length periodic focusing IMS drift cell. The drift cell is operated at a pressure of ~1 torr, using helium as the buffer gas. A non-uniform electric field is established along the length of the drift cell by applying a voltage (1900 V) across a chain of 1 MΩ resistors [32]. Ions exiting the drift cell are accelerated to 80–120 eV by the last plate of the mobility cell, pass through a differentially pumped region (from 1 to $\sim 10^{-5}$ torr), and then are focused by a five-element lens into an orthogonal extraction SID/TOF source (10^{-7} torr). The ions entering the TOF source can be extracted and mass analyzed or allowed to collide with a surface and then mass analyzed by TOF. TOF data is collected using a multi-channel time-to-digital converter (TDC, Ionwerks, Houston TX), and the data is monitored using a 2-D acquisition software specifically designed for the IM-MS experiment (Ionwerks, Houston, TX). Both 1-D and 2-D spectra are displayed using a customized data processing software (Ionwerks, Houston, TX) produced with the IDL language (Research Systems, Boulder, CO).

The SID/TOF source (Fig. 2) consists of three stainless steel plates (40 mm × 40 mm × 0.635 mm, eV parts, Kimball Physics Inc.) and a stainless steel ring electrode (25 mm i.d., 6.35 mm thick) that is sandwiched between the middle and bottom plates. Each of the top two plates has a 20 mm opening that is covered with a 90% transmission grid (30 lines/cm, Precision Eforming) to allow maximum ion transmission. These three plates are separated by 2 mm (top to middle) and 8 mm (middle to bottom), respectively, to form a Wiley–McLaren type TOF source. Ions exiting the mobility drift cell enter the extraction source assembly through a small hole (3.8 mm i.d.) in the ring electrode. The potentials applied to the ring electrode and the two plates are modulated to allow the ions to traverse the source to the collision surface or be extracted into the TOF mass analyzer prior to SID. Fig. 3 shows the sequence of this modulation process. Voltages of +1.2, +1.35, and +1.5 kV are applied to the middle plate, ring, and bottom plate, respectively, during the extraction time (the top plate is always grounded and +1.35 kV on the ring electrode is for keeping a linear electric field in the source), and only +1.5 V is applied to the ring (all other electrodes are kept grounded) between pulses. The ions that traverse the SID/TOF source are subjected to collisions with the inner wall (stainless steel surface) of the ring electrode, and low energy ions scattered by ion–surface collisions are confined by the trapping well defined by the small bias voltage. SIMION 7.0 (Idaho National Engineering and Environmental Laboratory, Idaho Falls, ID) was used to simulate ion trajectories in the source and to model

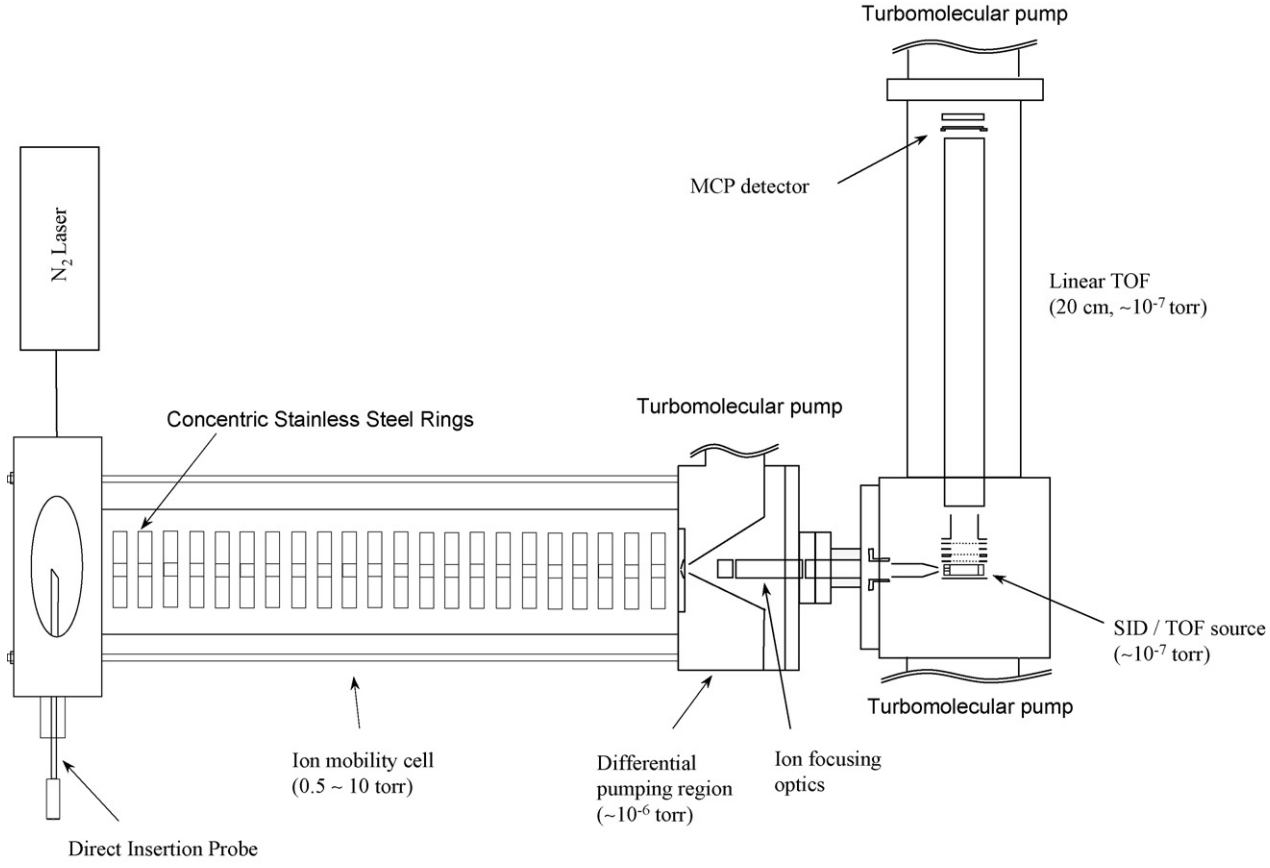

Fig. 1. Schematic diagram of the MALDI-IM-SID-oTOF instrument.

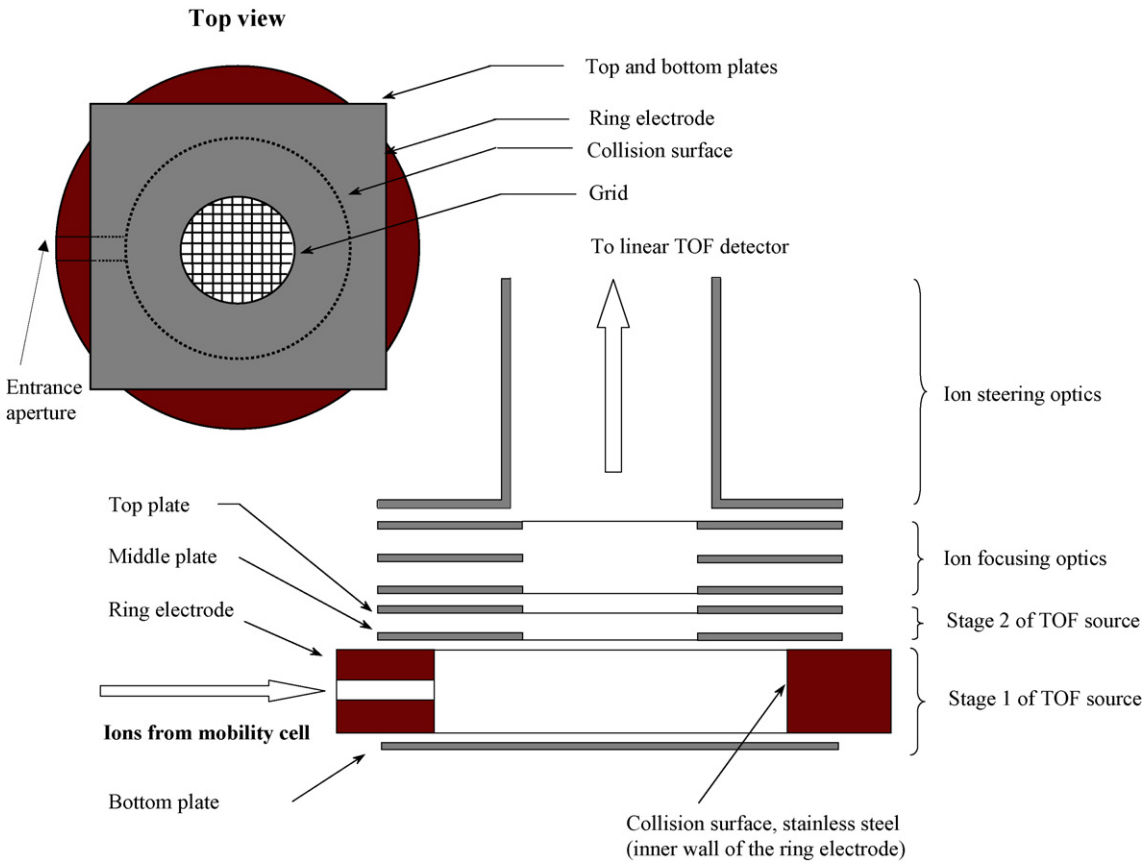

Fig. 2. Schematic diagram of the SID/TOF source region. The inset at the upper left shows the top view of the source region excluding the ion focusing and steering optics.

the relationship between bias voltages and ion abundances for SID formed fragment ions.

Note that for the studies reported here the SID surface is made of stainless steel, and the vacuum pumping system is a dry system composed of turbo-molecular pumps and oil-free scroll pumps. No special efforts have been made to clean the stainless steel surface by sputtering or other techniques, thus the SID surface is actually an overlayer of adsorbed species, such as organic material and water.

The peptide RVGVAPG (654.8 *m*/*z*) was synthesized in house using Fmoc chemistry on solid support [33]. The peptides des-Arg^9-bradykinin (RPPGFSPF, 903.4 *m*/*z*), angiotensin I (DRVYIHPFHL, 1295.7 *m*/*z*), and angiotensin II (DRVYIHPF, 1045.5 *m*/*z*) were acquired from Sigma (St. Louis, MO).

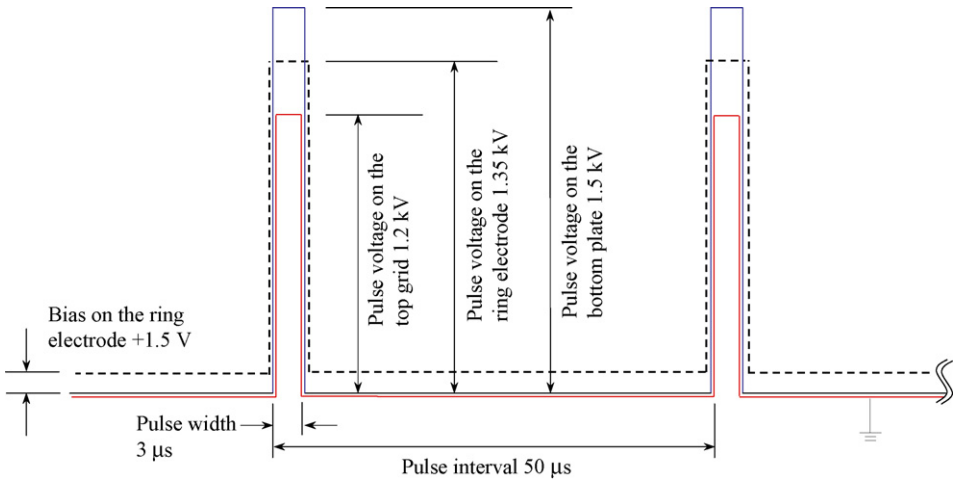

Fig. 3. The timing sequence and amplitudes of the pulse signals during the SID process and TOF extractions. Note that all three pulse signals are concurrent and the bias voltage (+1.5 V) is applied to the ring electrode.

Gramicidin S (cyclic-OLFPVOLFPV, 1141.5 *m*/*z*) and a linear analogue of gramicidin S (OLFPVOLFPV, 1159.5 *m*/*z*) were acquired from Enanta Pharmaceuticals Inc. (Watertown, MA). All of the peptides were used without further purification. α-Cyano-4-hydroxycinnamic acid was acquired from Sigma and recrystallized. The standard dried droplet MALDI sample preparation technique was used with a 1000:1 matrix-to-analyte ratio.

3. Results and discussion

A complete understanding of SID processes, i.e., energy uptake as a result of ion–surface collisions and how chemical and physical properties of the surface affect such processes, requires precise control of many experimental parameters (e.g., the incident angle and incident energy of the ions), whereas the analytical utility of SID is directly dependent upon the efficiency of precursor and fragment ion sampling. Consequently, we have focused our efforts on designing an SID apparatus that will allow for efficient SID as well as high collection efficiency of the SID fragment ions. Owing to parameters such as the operating pressure of the IM drift cell (1–10 torr) and the distance between the exit of the drift cell and the orthogonal TOF source, we have added a differential pumping stage and ion focusing optics between these components. The ions exiting the ion mobility drift cell must traverse the SID/TOF source before striking the collision surface (Fig. 2). Thus, in our experiment SID is performed using zero incident angle or "normal mode" collisions. Cooks and Wysocki estimated that 1–10% of the incident ions that undergo collisions with the surface at a 45° incident angle produce detectable fragment ions [34,35], and Laskin has suggested comparable SID efficiencies for "surface-normal mode" experiments [20]. The most significant difference between the 45° incidence and surface-normal incidence experiments is the kinetic energy of the scattered ions, i.e., Laskin observed kinetic energy of less than 1 eV for peptide ions scattered from a self-assembled monolayer surface in a surface-normal incidence collision [20] as compared with up to 10 eV (40% of the incident energy) observed by Cooks using a 45°incident angle [17,23]. Ions with such small kinetic energies will be easily diverged owing to a number of factors, i.e., inhomogeneous electric fields and ion space charge effects [36]; however, ion divergence can be minimized by post acceleration of the SID fragments [37,38] or by utilizing an electrostatic lens to focus the ions into the TOF source [18].

We have explored the use of parallel plates and a dc biased ring-electrode to confine the scattered ions before they are extracted towards the TOF detector. Ion confinement is achieved by applying an electrostatic potential to the ring-electrode to establish a potential well between two parallel plates (see below). Considering the SID survival rate (e.g., 1–10%) [34,35] and the extraction efficiency of the source (i.e., ion residence time in the source vs. time interval between extraction pulses), 0.3–3% of the total incident ions are estimated to be finally detected with TOF. Of course, the actual number of ions that are scattered from the SID surface depends upon the collision energy and the composition of the surface. If we assume that the number of ions formed by MALDI (20 Hz N_2 laser) is around 10^5 per laser shot [39] and the mobility cell transmission is conservatively about 10% [32], we estimate fragment ion count rates of 60–600 s^{-1} are available to be detected, and these estimates compare favorably with the experimental data.

SIMION was used to model the scattered ion trajectories (see Fig. 4). In the simulation the kinetic energy of the scattered ion beam is assumed to be 1.5 eV and the angular distribution of the beam is assumed to be 40°, based upon the results for small organic ions colliding at the 45° incident angle [40,41]. A larger angular distribution (∼90°) was observed by Kleyn and co-workers at the normal incident angle; however, these investigations involved exclusively very small ions (e.g., K^+) on clean crystal surfaces (e.g., W(1 1 0)) [25]. The middle column of Fig. 4 represents the top views (looking into the ring) of the scattered ion trajectories at the different bias voltages on the ring electrode, and the right column represents the corresponding side views of these trajectories. Fig. 4 (left column) contains two potential energy views for bias voltages of +1.5 and −1.5 V on the ring electrode, respectively. A potential hill is established for positive ions when the bias voltage on the confinement ring is negative in the potential energy view (the top and bottom plates are grounded throughout the experiment). This potential hill leads to ion spread on the plane parallel to the source plate (see the potential energy view for the bias −1.5 V on the left column of Fig. 4) or even withdrawing to the collision site on the ring electrode (see the top view for the bias −2 V on the middle column of Fig. 4) due to the small kinetic energy the scattered positive ions have. Applying a small positive voltage on the ring electrode creates a potential well that helps confine the scattered ions to the central axis of the TOF source (e.g., the potential energy view for the bias +1.5 V on the left column of Fig. 4); however, when higher positive voltages (e.g., +5 V) are applied to the ring electrode the ions will be accelerated so that they do not enter the linear TOF detector which is located 20 cm directly above the source. Fig. 5 contains plots of total ion abundances versus applied ring electrode bias voltages for the simulated and experimental data. The simulated data (● points in the plot) shows a rapid increase of the total scattered ion intensity from ∼ −1.5 to ∼ +1.5 V. The experimental data (SID spectra shown as inserts in Fig. 5 and ▲ points in the plot) shows a similar trend that the ion abundances are low at small negative bias voltages, but the ion abundances increase as the voltage is increased from ∼ −1.5 to ∼ +1.5 V. Note that the resolution of the SID spectra changes significantly across this same range of voltages. Also, the simulation assumes that the kinetic energy of the scattered ions is small (∼1.5 eV). This assumption is supported by the close correlation between the simulated curve and the experimental curve. It is also consistent with the result reported by Futrell and co-workers where less than 1 eV kinetic energy for the scattered ions was measured in their surface-normal impact SID experiments [20].

The SID/TOF source was critically evaluated using a series of peptides. Fig. 6a and b contain SID spectra for RVGVAPG $[M+H]^+$ ions (75 eV impact energy) and des-Arg^9-bradykinin $[M+H]^+$ ions (90 eV impact energy), respectively. The spectra are similar to both CID and SID spectra reported previously

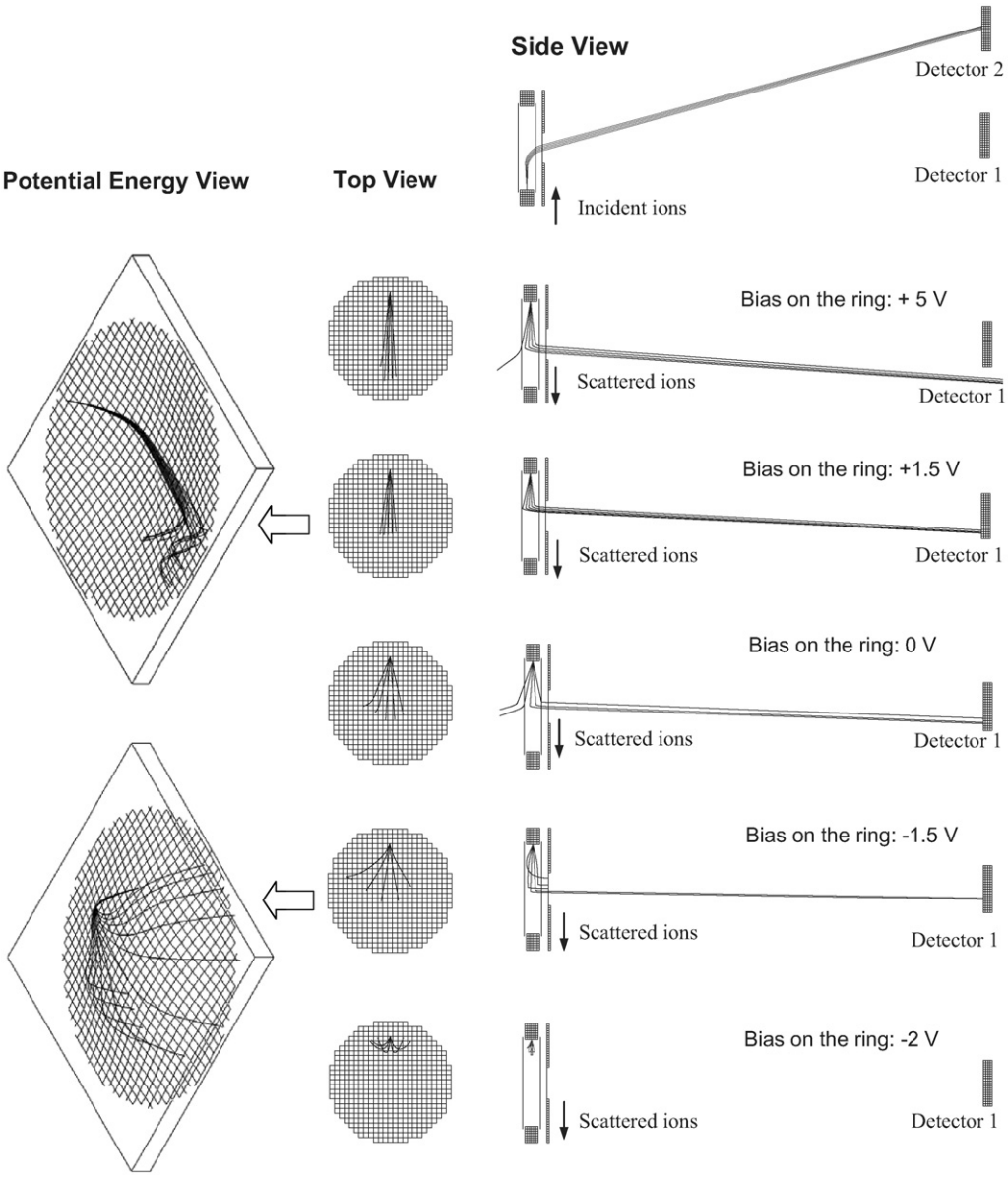

Fig. 4. Simulated ion trajectories (by SIMION 7.0) at the different bias voltages on the ring electrode. The right column represents the side views of the SID/TOF source and the TOF flight region (note that detector 2 at the upper right corner is not a part of the current instrument and it is added for illustrating that it is possible in the future to simultaneously detect both the incident and scattered ions in a single experimental sequence); the middle column represents the top views of the SID/TOF source region; the left column represents the potential energy views of the source region at the bias voltages of +1.5 and −1.5 V, respectively. The assumed initial kinetic energy of incident and scattered ions are 100 and 1–2 eV, respectively; *m/z*: 1000; assumed angular distribution: 40°.

[31,42]. That is, the spectra contain a complete series of both a- and b-type fragment ions, several y-type fragment ions, and ions formed by loss of small neutral molecules such as water and ammonia. Due to the short flight times and the low extraction voltages used in these studies, the mass resolution for each mass spectrum shown in this work is around 100, therefore no isotopic distribution of precursor peaks is resolved. CID spectra acquired for the same peptides on an Applied Biosystems 4700 TOF/TOF instrument have similar fragmentation patterns, except that the high mass fragments have higher ion abundances in the CID case, which is presumably due to either less kinetic energy applied in the laboratory frame or a lower conversion efficiency (translational → vibrational), or both in the CID experiment [42]. Compared with the gold mesh in-line SID data acquired previously in our group (in this experiment an ion beam is passed through a series of gold mesh layers to induce a grazing angle SID) [30], the increased sensitivity over that observed and our previous SID studies is primarily attributed to the fact that almost all the ions strike the surface in the surface-normal incidence collision whereas as much as 80% of the ion beam in the in-line experiments passes through the multi-layer gold mesh system completely [30]. Additionally, the trajectories of the ions emerging from the gold mesh is much less predictable and therefore the collection efficiency is relatively low.

Fig. 6c and d contain SID mass spectra of gramicidin S (cyclic) and a linear analog (OLFPVOLFPV), respectively. In

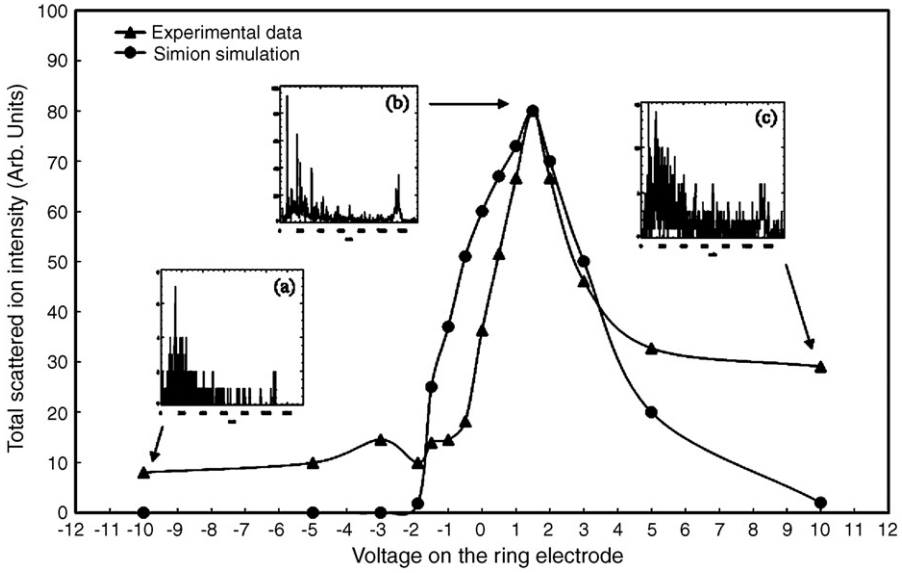

Fig. 5. Total scattered ion intensity of gramicidin S as a function of the bias voltage on the ring electrode. Triangles represent the experimental data. Circles represent the results from SIMION simulation. Mass spectra obtained at bias voltages (a) −10 V, (b) +1.5 V, and (c) +10 V.

the case of gramicidin S, most of the fragments are proline terminated due to the so called proline effect (preferred cleavage of peptide bond between proline and adjacent amino acid [43]). This fragmentation pattern is similar to those obtained from a 45° incidence collision at the same impact energy (90 eV). The primary difference between the 45° and the surface-normal modes is that the abundances of the low mass fragments are relatively higher in the normal incidence collision, most likely because the energy deposition efficiency in the surface-normal incidence collision is higher. Since the energy deposition efficiency of both the 45° incidence collision and the grazing-incidence collision have been reported to have similar values on stainless steel surfaces [35], it can be assumed that the energy deposition efficiency of the normal incidence collision is also higher than that of the grazing-incidence collision (there is no direct comparison yet between the normal and grazing incidence SID in the same instrument for the same type of surface). At 80 eV impact energy a near complete series of both b- and y- type fragment ions of the gramicidin S linear analog (OLFPVOLFPV) are observed as well as several internal fragments. Similar to the gramicidin S example, more low mass fragments were observed for the gramicidin S linear analog in the normal incidence collision than in the 45° incidence collision [44]. Increasing the impact energy in the 45° incidence collision mode to match the amount of energy deposited by the normal incidence collision will sacrifice mass resolution, since the velocity spread of the scattered ions on the axis of the TOF pulse extraction will increase accordingly in the 45° incidence collision mode.

Ratios of fragment ions to $[M+H]^+$ abundances for surface-normal impact and 45° impact angles are summarized in Table 1. At the same impact energy all of the peptides show a higher fragment ion abundance for the surface-normal impact SID mode (shown as a lower ratio), which further confirms the conclusion drawn for gramicidin S and its linear analog (OLFPVOLFPV).

Since the ion mobility drift time (hundreds of μs to ms) is much greater than the time required to acquire a TOF mass spectrum (10–100 μs), coupling these two techniques with a fragmentation step such as SID can avoid interrogating each intact analyte ion individually as required by other tandem MS techniques. That is, the information for peptide mass mapping and peptide sequencing can be achieved simultaneously in a single experiment sequence to significantly enhance the sequencing throughput, as illustrated in Fig. 7. It should also be noted that another advantage of IM-SID-MS over conventional MS–MS experiments is that the IM-SID-MS data can be acquired in both data-dependent and non-data-dependent modes. Using conventional tandem MS techniques sorting of non-data-dependent data is difficult, whereas the association of fragment ions and precursor ions is preserved in the 2-D IM-MS data projection. In addition, a mobility resolution of 20 provides sufficient separation of the two peptides for unambiguous correlation of fragment ions. The peak tailing to longer drift times for the angiotensin I mobility peak in Fig. 7 is due to matrix-analyte cluster ions, which survive the MALDI event but dissociate upon SID to form angiotensin I $[M+H]^+$ ions. This phenomenon had been observed previously for peptides, dendrimers, DNA-metal ion complexes, and other highly polar molecules by Stone et al. [31]. The abundances of these cluster ions can be minimized by imparting sufficient energy to the ions to decluster them in the MALDI source.

Table 1
Ratio of integrated area of precursor ion to the sum of integrated areas for all fragment ions[a]

SID configuration/peptides	des-Arg^9-bradykinin	Gramicidin S	Substance P
Surface-normal impact	1:12.5	1:6.9	1:2.7
45° impact [31]	1:11	1:2.7	1.4:1

[a] Stainless steel surface with 90 eV impact energy.

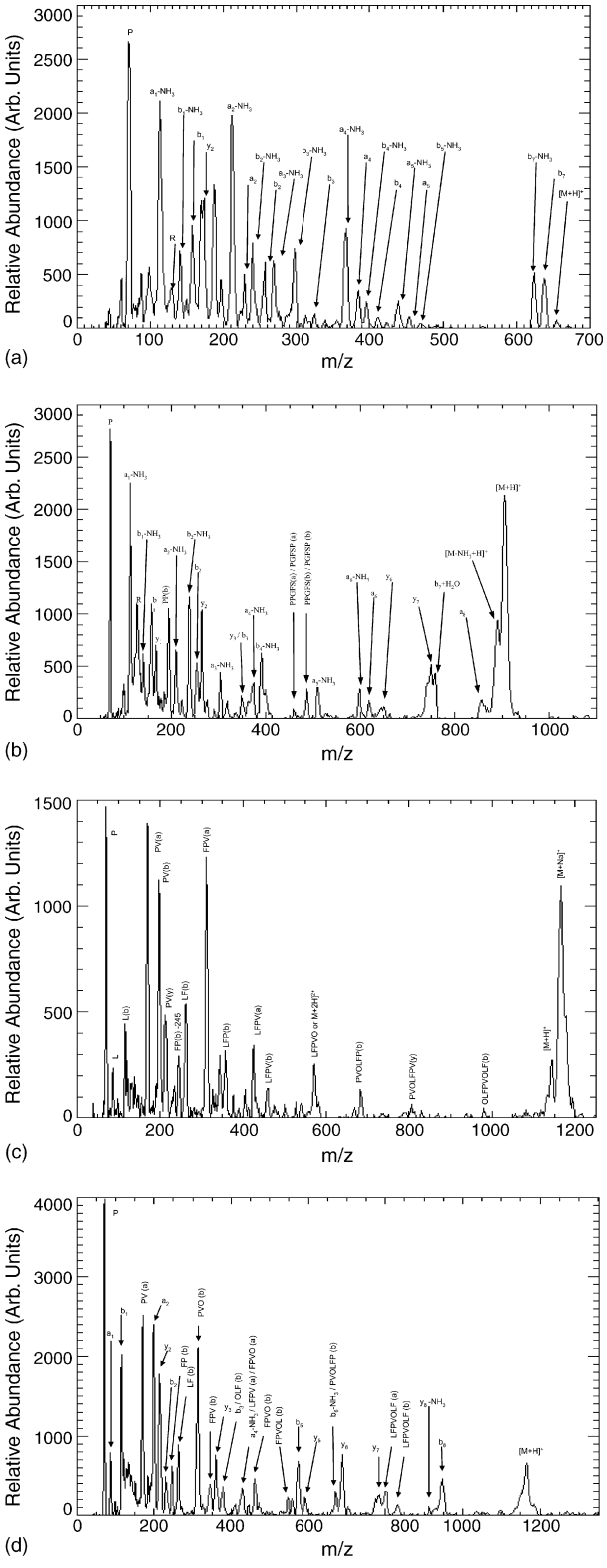

Fig. 6. MALDI-SID-oTOF mass spectra of RVGVAPG (654.8 *m/z*) at collisional energy ~75 eV (a), des-Arg^9-bradykinin (RPPGFSPF, 903.4 *m/z*) at collisional energy ~90 eV (b), gramicidin S (cyclic-OLFPVOLFPV, 1141.5 *m/z*) at collisional energy ~90 eV (c), and gramicidin S linear analog (OLFPVOLFPV, 1159.5 *m/z*) at collisional energy ~80 eV (d). Mass accuracy for labeled SID fragments is ± 1 amu. Mass resolution is ~100. The bias voltage on the ring electrode is +1.5 V.

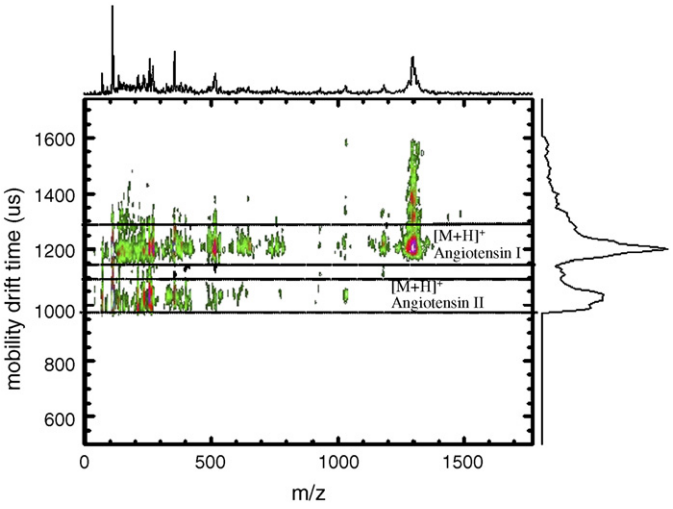

Fig. 7. A mobility-mass spectrum of two-peptide mixture (angiotensin I (DRVYIHPFHL, 1295.7 *m/z*) and angiotensin II (DRVYIHPF, 1045.5 *m/z*)) acquired at collisional energy ~120 eV. The bias voltage on the ring electrode is +1.5 V.

4. Conclusions

The new SID/TOF source configuration discussed here provides three primary functions: (i) it provides a surface for the normal incident collision, (ii) by pulsing the ring electrode simultaneously with the TOF extraction plates, it maintains linearity of the field in a large collection space to accommodate the diverged scattered ions, and (iii) it helps confine the scattered ions by establishing an electrostatic potential well within the ring electrode. This new in-line SID source provides a convenient way to directly couple an MS1 stage to an orthogonal TOF mass spectrometer either in a home-built or a commercial instrument. Other existing in-line SID devices all share common limitations, such as relatively small energy deposition efficiency due to the grazing incident angle used and low sensitivity caused by poor ion collection efficiency [31,35]. The current instrument circumvents these limitations by utilizing a surface-normal incident angle and by performing the SID within the TOF extraction source. This surface-normal impact design also simplifies the ion optics compared with the slant plate or cone-cylinder design [35], because the collision area and the scattered angle in this design are no longer dependent upon the incident kinetic energy. The SID efficiency of this instrument has not yet been critically evaluated, but more than an order of magnitude improvement has been observed when compared with the gold mesh SID experiment previously performed in our laboratory [31]. Furthermore, the normal incidence collision mode also overcomes some limitations of the 45° incidence collision SID such as the relatively large kinetic energy distribution of the scattered ions and the various scattering angles for different scattered ions and different surfaces (such limitations can affect both the resolution and sensitivity of the SID experiment).

Acknowledgements

Financial support for this work was provided by U.S. Department of Energy, Division of Chemical Sciences (BES

DE-FG02-04ER15520) and the Robert A. Welch Foundation (A-1176).

References

[1] C.M. Whitehouse, R.N. Dreyer, M. Yamashita, J.B. Fenn, Anal. Chem. 57 (1985) 675.
[2] M. Karas, D. Bachmann, U. Bahr, F. Hillenkamp, Int. J. Mass Spectrom. Ion Process. 78 (1987) 53.
[3] K. Tanaka, H. Waki, Y. Ido, S. Akita, Y. Yoshida, T. Yoshida, Rapid Commun. Mass Spectrom. 2 (1988) 151.
[4] W.J. Henzel, T.M. Billeci, J.T. Stults, S.C. Wong, C. Grimley, C. Watanabe, Proc. Natl. Acad. Sci. USA 90 (1993) 5011.
[5] D.N. Perkins, D.J. Pappin, D.M. Creasy, J.S. Cottrell, Electrophoresis 20 (1999) 3551.
[6] K. Biemann, Meth. Enzymol. 193 (1990) 455.
[7] K.R. Jennings, Int. J. Mass Spectrom. Ion Phys. 1 (1968) 227.
[8] W.F. Haddon, F.W. McLafferty, J. Am. Chem. Soc. 90 (1968) 4745.
[9] N.J. Jensen, M.L. Gross, Mass Spectrom. Rev. 6 (1987) 497.
[10] R.G. Cooks, D.T. Terwilliger, T. Ast, J.H. Beynon, T. Keough, J. Am. Chem. Soc. 97 (1975) 1583.
[11] M.A. Mabud, M.J. Dekrey, R.G. Cooks, 67 (1985) 285.
[12] F.M. Harris, J.H. Beynon, in: M.T. Bowers (Ed.), Gas Phase Ion Chemistry, vol. 3, Academic Press, Orlando, 1984, p. 99.
[13] R.C. Dunbar, in: M.T. Bowers (Ed.), Gas Phase Ion Chemistry, vol. 3, Academic Press, Orlando, 1984, p. 129.
[14] D.C. Barbacci, D.H. Russell, J. Am. Soc. Mass Spectrom. 10 (1999) 1038.
[15] R.A. Zubarev, N.L. Kelleher, F.W. McLafferty, J. Am. Chem. Soc. 120 (1998) 3265.
[16] J.E.P. Syka, J.J. Coon, M.J. Schroeder, J. Shabanowitz, D.F. Hunt, P. Natl., Acad. Sci. USA 101 (2004) 9528.
[17] M.R. Morris, D.E. Riederer Jr., B.E. Winger, R.G. Cooks, T. Ast, C.E.D. Chidsey, Int. J. Mass Spectrom. Ion Process. 122 (1992) 181.
[18] R. Worgotter, J. Kubista, J. Zabka, Z. Dolejsek, T.D. Mark, Z. Herman, Int. J. Mass Spectrom. Ion Process. 174 (1998) 53.
[19] D.G. Schultz, H. Lim, S. Garbis, L. Hanley, J. Mass Spectrom. 34 (1999) 217.
[20] J. Laskin, J.H. Futrell, Mass Spectrom. Rev. 24 (2005) 135.
[21] O. Meroueh, W.L. Hase, J. Am. Chem. Soc. 124 (2002) 1524.
[22] G. Schultz, S.B. Wainhaus, L. Hanley, P. de Sante Claire, W.L. Hase, J. Chem. Phys. 106 (1997) 10337.
[23] V. Grill, J. Shen, C. Evans, R.G. Cooks, Rev. Sci. Instrum. 72 (2001) 3149.
[24] J. Laskin, J.H. Futrell, Mass Spectrom. Rev. 22 (2003) 158.
[25] A.D. Tenner, K.T. Gillen, T.C.M. Horn, J. Los, A.W. Kleyn, Surf. Sci. 172 (1986) 90.
[26] E.R. Williams, G.C. Jones Jr., L. Fang, R.N. Zare, B.J. Garrison, D.W. Brenners, J. Am. Chem. Soc. 114 (1992) 3207.
[27] E.R. Williams, L. Fang, R.N. Zare, Int. J. Mass Spectrom. Ion Process. 123 (1993) 233.
[28] B.E. Winger, R.K. Julian Jr., R.G. Cooks, C.E.D. Chidsey, J. Am. Chem. Soc. 113 (1991) 8967.
[29] V.H. Wysocki, J.L. Jones, J. Ding, J. Am. Chem. Soc. 113 (1991) 8969.
[30] E.G. Stone, K.J. Gillig, B. Ruotolo, K. Fuhrer, M. Gonin, A. Schultz, D.H. Russell, Anal. Chem. 73 (2001) 2233.
[31] E.G. Stone, K.J. Gillig, B.T. Ruotolo, D.H. Russell, Int. J. Mass Spectrom. Ion Process. 212 (2001) 519.
[32] K.J. Gillig, B.T. Ruotolo, E.G. Stone, D.H. Russell, Int. J. Mass Spectrom. Ion Process. 239 (2004) 43.
[33] J.G. Slaton, W.K. Russell, D.H. Russell, J. Am. Chem. Soc., in press.
[34] R.G. Cooks, T. Ast, M.A. Mabud, Int. J. Mass Spectrom. Ion Process. 100 (1990) 209.
[35] V.H. Wysocki, J.M. Ding, J.L. Jones, J.H. Callahan, F.L. King, J. Am. Soc. Mass Spectrom. 3 (1992) 27.
[36] K.L. Busch, Spectroscopy 19 (2004) 35.
[37] E.R. Williams, G.C. Jones Jr., L. Fang, R.N. Zare, B.J. Garrison, D.W. Brenners, J. Am. Soc. Mass Spectrom. 114 (1992) 3207.
[38] E.N. Nikolaev, A. Somogyi, D.L. Smith, C. Gu, V.H. Wysocki, C.D. Martin, G.L. Samuelson, Int. J. Mass Spectrom. Ion Process. 212 (2001) 535.
[39] K. Dreisewerd, Chem. Rev. 103 (2003) 395.
[40] R. Wörgötter, J. Kubišta, J. Žabka, Z. Dolejšek, T.D. Mark, Z. Herman, Int. J. Mass Spectrom. 174 (1998) 53.
[41] A.K. Shukla, J.H. Futrell, Int. J. Mass Spectrom. 228 (2003) 563.
[42] J.W. Morgan, J.M. Hettick, D.H. Russell, Meth. Enzymol. 402 (2005) 186.
[43] J.A. Loo, C.G. Edmonds, R.D. Smith, Anal. Chem. 65 (1993) 425.
[44] E.G. Stone, Ph.D Thesis Texas A&M University, 2003.